Using linear spectral unmixing of high spatial resolution and hyperspectral data for geometric-optical modelling

Zeng, Yuan ; Schaepman, Michael E ; Wu, Bingfang ; Clevers, Jan G P W ; Bregt, Arnold K

Abstract: The linear spectral mixing model is a widely used technique in remote sensing to estimate the fractions of several individual surface components present in an image pixel and the pure reflectance spectrum of a component, called endmember, is the model's necessary parameter. Different methods can be used to extract endmembers, finding out the pure pixel from hyperspectral data is the most common way, but at the regional scale, the selected single pixel can not present the typical component accurately. The objective of this paper is to estimate the feasibility of up-scaling from high spatial resolution data to medium spatial resolution hyperspectral data by linear spectral unmixing based technique for extracting the required endmembers. In this case, an inverted Li-Strahler geometric-optical model is applied to retrieve one of the forest canopy variables (crown closure) in a broadleaved forest natural reserve, located in the Three Gorges region of China. This model needs three important scene components (sunlit canopy, sunlit background and shadow). The three components' classes are firstly estimated using QuickBird fusional image with 0.6 m spatial resolution by eCognition, an object-based classification method. Then, a 50 by 50 pixels moving window calculated each component's proportion is matched to individual pixels with 30 m spatial resolution of EO-1 Hyperion data. The umixing model is finally used for deriving the three endmembers based on the Hyperion data with surface reflectance and the per-pixel three fractions computing from QuickBird classification. From the spectral profile comparison, the scaling-based endmembers indicate the mean spectra of the components unlike the pure pixels' spectra. For validating the results, we use 32 independent sample sites collected in the study area to assess the accuracy of inverted model's outputs, and the results of scaling-based endmember extraction method (R^2=0.60) seem better than the pixel-based method (R^2=0.51).

Originally published at:
Zeng, Yuan; Schaepman, Michael E; Wu, Bingfang; Clevers, Jan G P W; Bregt, Arnold K (2007). Using linear spectral unmixing of high spatial resolution and hyperspectral data for geometric-optical modelling. In: Int. Symposium on Physical Measurements and Spectral Signature in Remote Sensing, Davos, Switzerland, 12 March 2007 - 14 March 2007. ISPRS, 304-309.

USING LINEAR SPECTRAL UNMIXING OF HIGH SPATIAL RESOLUTION AND HYPERSPECTRAL DATA FOR GEOMETRIC-OPTICAL MODELLING

Yuan Zeng [a, b, *], Michael E. Schaepman [a], Bingfang Wu [b], Jan G.P.W. Clevers [a], Arnold K. Bregt [a]

[a] Centre for Geo-Information, Wageningen University and Research Centre, the Netherlands - (yuan.zeng, michael.schaepman, jan.clevers, arnold.bregt)@wur.nl
[b] Institute of Remote Sensing Applications, Chinese Academy of Sciences, China – (yuanz, wubf)@irsa.ac.cn

KEY WORDS: Linear spectral mixing model, EO-1 Hyperion, QuickBird, Geometric-optical model, Forest canopy variables

ABSTRACT:

The linear spectral mixing model is a widely used technique in remote sensing to estimate the fractions of several individual surface components present in an image pixel and the pure reflectance spectrum of a component, called endmember, is the model's necessary parameter. Different methods can be used to extract endmembers, finding out the pure pixel from hyperspectral data is the most common way, but at the regional scale, the selected single pixel can not present the typical component accurately. The objective of this paper is to estimate the feasibility of up-scaling from high spatial resolution data to medium spatial resolution hyperspectral data by linear spectral unmixing based technique for extracting the required endmembers. In this case, an inverted Li-Strahler geometric-optical model is applied to retrieve one of the forest canopy variables (crown closure) in a broadleaved forest natural reserve, located in the Three Gorges region of China. This model needs three important scene components (sunlit canopy, sunlit background and shadow). The three components' classes are firstly estimated using QuickBird fusional image with 0.6 m spatial resolution by eCognition, an object-based classification method. Then, a 50 by 50 pixels moving window calculated each component's proportion is matched to individual pixels with 30 m spatial resolution of EO-1 Hyperion data. The umixing model is finally used for deriving the three endmembers based on the Hyperion data with surface reflectance and the per-pixel three fractions computing from QuickBird classification. From the spectral profile comparison, the scaling-based endmembers indicate the mean spectra of the components unlike the pure pixels' spectra. For validating the results, we use 32 independent sample sites collected in the study area to assess the accuracy of inverted model's outputs, and the results of scaling-based endmember extraction method (R^2=0.60) seem better than the pixel-based method (R^2=0.51).

1. INTRODUCTION

At local to regional and global scales, remote sensing has facilitated extraordinary advances in the modelling, mapping, and understanding of ecosystems and their functioning. One basic characteristic of remote sensing in the twenty-first century is the extensive use of quantitative algorithms for estimating Earth surface variables (Liang, 2004). Forests, being one of the most important natural resources worldwide, not only regulate the global atmospheric cycles, but also are increasingly being used in dynamic global vegetation models for terrestrial CO_2 estimations.

A lot of work in monitoring forest canopy variables using remote sensing has focussed on inverting physical based canopy reflectance models. Geometric-optical models, which treat the surface as an assemblage of discrete geometric objects with the reflectance modelled as a linear combination of viewed sunlit and shaded components, have been used successfully to estimate the forest canopy (Chopping et al., 2006; Franklin and Strahler, 1988; Gemmell, 1999; Gerard and North, 1997; Hall et al., 1995; Peddle et al., 2003; Peddle et al., 1999; Scarth and Phinn, 2000; Scarth et al., 2001; Woodcock, 1994; Woodcock et al., 1997). The accuracy of the inverted model's results is primarily related to the model inputs. In a previous study, we derived forest crown closure and crown diameter by inverting the Li-Strahler geometric-optical model (Zeng et al., 2007), one of the most important inputs is the fractional image of one scene component–sunlit background, which was calculated based on the pure reflectance spectra of viewed surface components, called endmembers. Therefore, the method and certainty of the endmember extraction is the main factor to influence the value of the inverted Li-Strahler geometric-optical model.

Different approaches can be used to extract endmembers, like deriving the pure spectrum from the image with field training samples, directly obtaining from the observation of a field spectrometer or from an existing spectral library. For extracting the endmembers of sunlit and shaded scene components by hyperspecral remote sensing data, the most common way is selecting the pure pixels from the image. However, due to the spatial resolution of hyperspectral imagery, the "pure" pixel may still contain mixtures of components, and also, at the regional scale, the selected single pixel can not present the typical component accurately. For solving this problem, a linear spectral mixing model is addressed. Zhukov et al. (1999) unmixed low-resolution images using the information about their pixel composition from co-registered high-resolution images. Haertel and Shimabukuro (2005) estimated the components' proportions from medium spatial resolution Landsat TM data and then successfully derived the unknown components' endmembers in the low spatial resolution Terra MODIS image by the linear spectral mixing model. Zurita-Milla et al. (2006) inverted the linear spectral mixing model to obtain MERIS endmembers based on the known fractional coverages of each pixel from a Landsat TM classification. In summary, when high spatial resolution imagery is available, the linear spectral mixing model can be used to unmix low spatial resolution data and estimate the required spectral reflectance. This method can also provide an avenue to up-scale the information from local to regional studies. Accordingly, the objective of this paper is to estimate the feasibility of up-scaling

* Corresponding author.

from high spatial resolution data to medium spatial resolution hyperspectral data by a linear spectral unmixing based technique for extracting the components' endmembers used for Li-Strahler geometric-optical modelling.

2. STUDY SITE

In this case, the study area, namely Longmenhe forest nature reserve, lies in the Xingshan county of Hubei province, towards the northeast of Three Gorges region in China (centred at 31°20′N, 110°29′E). The total reserve size is about 4644 ha. It is located in the temperate climate zone (Cwa–Subtropical monsoon, Koeppen (McKnight and Hess, 2000)) and is mainly dominated by natural evergreen broadleaved forest and mixed deciduous broadleaved forest. The field data were collected in June of 2003. A total of 40 sample sites (100mx100m) located in the study area were measured based on different plant strata and topographic distribution, and each of them randomly included 5 sample plots (20mx20m), which provided many field measurements about the forest canopy structure, such as crown closure, crown diameter, DBH (diameter at breast height), tree height, trunk height, tree age and visual estimations by forest experts for forest type, plant species and distribution. Those are the necessary ground truths for validating the model results.

3. METHOD

The overall method used in this study is shown as flowchart in Figure 1. The inverted Li-Strahler geometric-optical model is used to retrieve the forest canopy variables. The model needs three scene components: sunlit canopy (C), sunlit background (G) and shadow (T). The endmembers of these components are derived by two approaches:

- The G, C, T three components' classes are firstly estimated by a QuickBird fusional image with 0.6m spatial resolution using eCognition, an object-based classification method. Then, a 50 by 50 pixels moving window calculated each component's fraction is matched to individual pixels with 30m spatial resolution of EO-1 Hyperion image. The linear spectral mixing model is finally used for deriving the three endmembers based on the Hyperion data with surface reflectance and the per-pixel three fractions computing from QuickBird classification.
- Using the PPI algorithm to explore the pure pixel of each component directly from Hyperion hyperspectral image.

After inverting the model integrated with the components' endmembers, canopy structural parameters per forest class, and slope/aspect data, select one of the model outputs–forest crown closure to compare the two methods of endmember extraction, and make use of 32 measured field samples for validation.

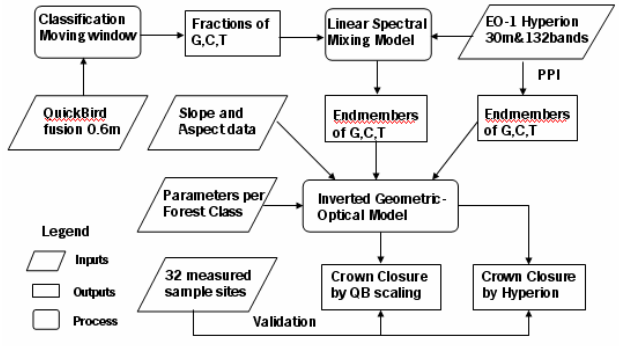

Figure 1. Flowchart of general method

3.1 Inverted Geometric-Optical Model

The Li-Strahler geometric-optical model (Li and Strahler, 1992; 1985) is based on the assumption that the Bidirectional Reflectance Distribution Function (BRDF) is a purely geometric phenomenon resulting from a scene of discrete three-dimensional objects being illuminated and viewed from different positions in the hemisphere. The reflectance associated with a given viewpoint is treated as an area-weighted sum of four fixed reflectance components: sunlit canopy, sunlit background, shaded canopy, and shaded background. Moreover, in most cases, these four components could be simplified to three: sunlit canopy–C, sunlit background–G and shadow–T (Li and Wang, 1995; Peddle et al., 2003; Peddle et al., 1999). This model also assumes that the resolution of the remote sensing image is much larger than the size of individual crowns but smaller than the size of forest stands, and that the individual trees are randomly (Poisson) distributed within the pixel (Woodcock et al., 1994). Based on the principle of three-dimensional geometry of a spherical crown on a flat background, each proportion of components can be expressed by a combination of the forest canopy structural parameters. For inverting the model, one of the components–sunlit background (Kg) can be used for deriving the expected forest crown closure (CC), see equations (1) to (5) (Li and Strahler, 1992; Strahler and Jupp, 1990; Woodcock et al., 1997).

$$K_g = e^{-\pi \cdot M \cdot [\sec(\theta_i)+\sec(\theta_v)-O(\theta_i,\theta_v,\varphi)]} \quad (1)$$

$$O(\theta_i,\theta_v,\varphi) = 1/\pi(\sec\theta_i + \sec\theta_v)(t - \sin t \cos t) \quad (2)$$

$$\cos t = \frac{h\left|\tan\theta_i - \tan\theta_v \cos\varphi\right|}{r(\sec\theta_i + \sec\theta_v)} \quad (3)$$

$$M = \frac{-\ln(K_g)}{(\sec\theta_i + \sec\theta_v)(\pi - t + \cos t \sin t)} \quad (4)$$

$$CC = 1 - e^{-\pi \cdot M} \quad (5)$$

Where, θ_i θ_v are the zenith angles of illumination and viewing, O is the average of the overlap function between illumination and viewing shadows of individual crowns as projected onto the background, φ is the difference in azimuth angle between illumination and viewing.

Since the study area is in the mountain region and actually the crown shape of the broadleaved forest needs to be modelled as an ellipsoid, with tree height (h) from ground to mid-crown, crown radius (b) in vertical direction and crown radius (r) in horizontal direction, double transformations are required to allow crowns to be treated as spheres and accommodate the sloping surface (Schaaf et al., 1994). The equations of all transformations are explained in Zeng et al. (2007).

Therefore, the required inverted model inputs for determining CC are the proportional image of Kg; the solar zenith and azimuth angles; the view zenith and azimuth angles; the local slope and aspect image and the mean measured parameters for different kinds of forest crown shapes: h, b, r. Among them, deriving the component fractional image of sunlit background is the most crucial process, which needs accurately extracting the endmembers of the three scene components.

3.2 Endmember Extraction

3.2.1 Linear Spectral Unmixing based technique

Traditionally, the linear spectral mixing model has been widely used to calculate the percentages of several individual surface components contained in each pixel of a remote sensing image (Goodwin et al., 2005; Peddle et al., 1999). The model assumes that the reflectance (S) of each pixel is a linear combination of endmembers (R), which are the pure reflectance spectra for each component. The general equations are:

$$S_j = \sum_{i=1}^{m} K_i R_{i,j} + v_j \qquad j = 1,2...,p \tag{6}$$

$$1 = \sum_{i=1}^{m} K_i \qquad K_i >= 0 \tag{7}$$

Where m is the number of components, in this case, m is the 3 components of C, G and T; p is the number of image bands; K is the fractional abundance of each component within the pixel and v is the residual for each band.

However, in this study, we use the inverted approach of this model, called linear spectral unmixing based technique. The fractions of each component within the pixel of a medium spatial resolution image are provided in advance from the overlapping high spatial resolution image, and then the endmembers of each component will be the final requirements. In practice, for deriving the endmembers, we need a test image with at least n pixels, and the number of n must be more than the number of components. Thus, equation (6) can be more conveniently expressed in matrix notation:

$$V_j = S_j - K * R_j \tag{8}$$

Vj: n-dimensional vector of the residuals in band j;
Sj: n-dimensional vector of the pixels' reflectance in band j;
K: n x m matrix of the fractions;
Rj: m-dimensional vector of the components' reflectance in band j.

We seek a set of numerical values for the unknowns in Rj such that the sum of the residual squares becomes minimum (9), and then the least squares solution for Rj can be shown in (10) (Haertel and Shimabukuro, 2005):

$$\frac{\partial(V_j' V_j)}{\partial R_j} = 0 \tag{9}$$

$$R_j = (K'K)^{-1} K' S_j \tag{10}$$

The three components' endmembers can be calculated after applying equation (10) to every spectral band in the medium spatial resolution hyperspectral image, and the inputs of this method are the fractional images for each components and a corresponding overlapped image with spectral reflectance.

3.2.2 PPI

The PPI (Pixel Purity Index) algorithm is a common method to find the most "spectrally pure" (extreme) pixels in multi-spectral and hyperspectral images. It is computed by repeatedly projecting n-dimensional scatterplots onto a random unit vector, and then the extreme pixels in each projection (those pixels that fall onto the ends of the unit vector) are recorded and the total number of times each pixel is marked as extreme is noted. That consists of the following steps (Plaza et al., 2004): 1. A "noise-whitening" dimensionality reduction step is performed by using the MNF (Minimum Noise Fraction) transform (Green et al., 1988). 2. A pixel purity score is calculated for each point in the image cube by randomly generating lines in the N-D space comprising the MNF transformed data. 3. All the points in that space are projected onto the lines, and the ones falling at the extremes of each line are counted. 4. After many repeated projections to different random lines, those pixels that count above a certain cut-off threshold are declared "pure". 5. These potential endmember spectra are loaded into an interactive N-D visualization tool and rotated in real time until a desired number of endmembers are visually identified as extreme pixels in the image. In this case, we use the PPI model of ENVI software to extract the components' endmembers directly from the hyperspectal data.

4. IMAGE DATA AND PROCESSING

For this study area, an EO-1 Hyperion image was acquired on June 10, 2004, around 11:00 a.m. local time. Hyperion, one of the three sensors on the NASA EO-1 platform, was launched on November 2000. As a push-broom imaging instrument, Hyperion provides images capable of resolving 242 spectral bands (from 0.4–2.5 μm) with a 10 nm spectral resolution and a 30m spatial resolution. For converting DNs to radiances, the data were scaled by 40 for VNIR and 80 for SWIR (Beck, 2003). Several stripes (data columns of poor quality) in the Hyperion data contain no information and lower radiance. Those abnormal pixels are detected and replaced by the average radiance value of their immediate left and right neighboring pixels (Han et al., 2002). In addition, an atmospheric correction is required. We use ACORN version 4.0, a commercially available atmospheric correction program based on the MODTRAN 4 radiative transfer code (AIG, 2002). Due to the low signal to noise ratio at the beginning and the end of the Hyperion spectra (≤436nm and ≥2385nm) and the heavy water absorption influences in several bands, a total of 64 bands are dropped from 196 valid bands. Geometric correction is done by 26 GCPs (Ground Control Points) relative to topographic maps and the geometric error is less than one pixel. Finally, the corrected Hyperion data with 132 bands of surface reflectance in a UTM Zone 49 N WGS-84 projection are used in this study.

The QuickBird data consisted of one panchromatic image at 0.61m resolution and one multi-spectral image with 4 spectral bands (B/G/R/NIR) at 2.44m resolution. It was collected on August 23, 2003 at 11:08 a.m. local time. This QuickBird image being the high spatial resolution data will be used together with Hyperion data to derive components' endmembers. Although the two images were acquired at different dates, the solar zenith and azimuth angles are similar (23.5° and 104.5° for Hyperion, 29.2° and 127.9° for QuickBird) and the sensor viewing direction is also the same at nadir. Hereby, only small variation in view/illumination geometry will be expected between the two images.

For classifying the three components from the QuickBird image and matching it to Hyperion data, we firstly merge the panchromatic and multi-spectral images by principal component method and cubic convolution resampling technique of ERDAS IMAGINE software, the output image includes 0.6m spatial resolution and 4 spectral bands. Then, an object-oriented classification software eCognition is carried out for classifying the components. eCognition is designed to segment the image into units of similar spectral and spatial patterns and to classify those segments according to a pre-defined rule base (Baatz et al., 2004). Finally, the geometrically corrected QuickBird fusional image being a base image is used to spatially co-register the two images, the matched subsets of Hyperion and QuickBird data that covered the same study region are selected.

5. RESULTS

5.1 Endmembers and Model Inputs

The processed Hyperion data with surface reflectance and 30m spatial resolution is shown in Figure 2a. The dimension of this image is 208 (column) x 173 (line) x132 (band). The fusional QuickBird image with 0.6m spatial resolution and 4 spectral bands (shown in Figure 2b) is located in the centre of Hyperion image, and it includes 4300 (column) x 3400 (line) pixels.

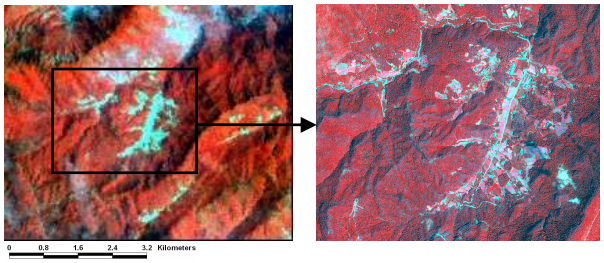

a. Hyperion image (bands: R50 G23 B16) b. QuickBird fusion image (R-NIR G-R B-G)

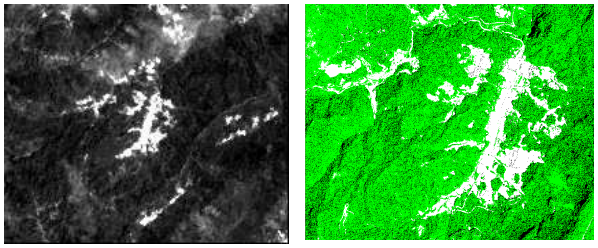

c. Proportional image of Kg (30m) d: Classification of QuichBird (0.6m)

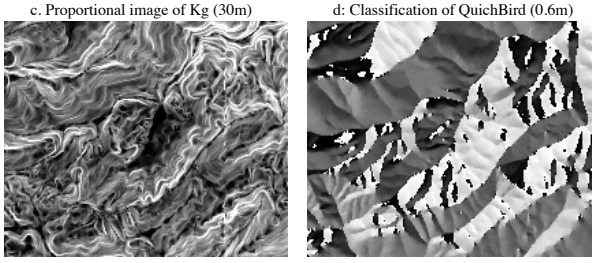

e. Slope data with 30m resolution f. Aspect data with 30m resolution

Figure 2: Processed Hyperion image, QuickBird image and the inputs of inverted Li-Strahler model

The three components classification result from the QuickBird fusional image by eCognition is shown in Figure 2d (White: G-sunlit background, Green: C-sunlit canopy and Black: T-shadow). After spatially co-registration, a subset of the Hyperion image with 86 (column) x 68 (line) is masked out for matching the QuickBird classification image. A 50x50 pixels moving window is used to calculate the fractions of each component from the QuickBird classification, and that is just matching the individual pixels of Hyperion data. Then the three components' endmembers extracted through the linear spectral unmixing based technique are shown in Figure 3. Comparing the endmembers retrieved from the pure pixels of the whole Hyperion image (G: x-104 y-89 C: x-150 y-102 T: x-127 y-117) by the PPI algorithm, the QuickBird scaling-based endmembers indicate the mean spectra of the components unlike the pure pixels' spectra.

In terms of the endmembers, the proportional images of Kg for both endmember extraction methods are derived by spectral unmixing the whole Hyperion image. Figure 2c illustrates one of the Kg images, which is from the QuickBird scaling-based endmembers. The brighter regions express higher proportions. The other required inputs for inversion of the Li-Strahler model, slope and aspect images with 30m spatial resolution are created from DEM data using topographic analysis model of ERDAS IMAGINE, see Figure 2e-f.

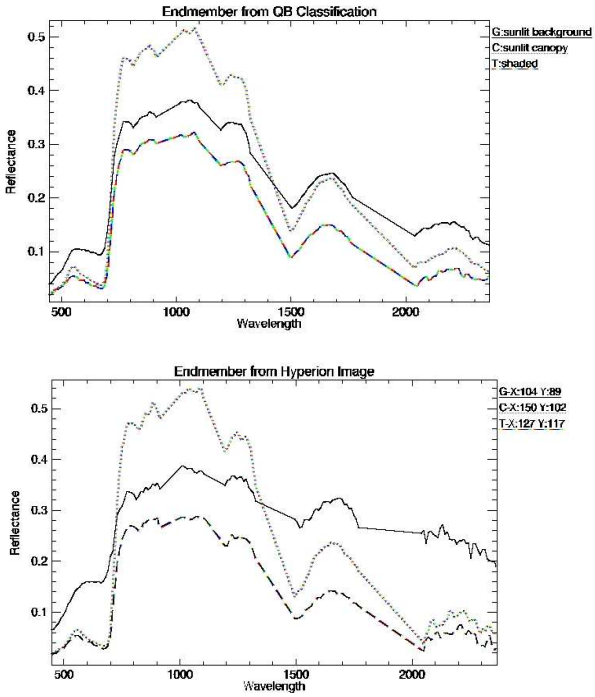

Figure 3: Components' endmembers (Up: QuickBird scaling-based method; Down: three pure pixels by PPI)

In this study area, the dominant forest communities include deciduous broadleaved forest, evergreen broadleaved forest, and conifer forest. Based on a forest classification image (Zeng et al., 2007) and the field measurements, the corresponding mean value of forest crown parameters, h, b, and r for every dominant forest class is shown in Table 1.

Dominant Forests	h (m)	b (m)	r (m)
Deciduous Broadleaved Forest	9.79	3.97	1.79
Evergreen Broadleaved Forest	8.86	3.36	1.61
Conifer Forest	8.41	4.63	1.51

Table 1. Inverted model inputs for each forest class

5.2 Model Outputs and Validation

We compiled an IDL program to implement the inversion of the Li-Strahler model integrated with the pixel-based inputs data. Figure 4 presents the final mapping results of forest crown closure distributed in the Longmenhe study area. The upper image is the model result according to the endmembers from the QuickBird scaling-based method and the other is the result for the PPI method. These two mapping images indicate the variety when one of the inverted model inputs (Kg) is different.

For validating the model outputs, we calculate the mean value of 3x3 pixels from the mapping image for comparison to one field sample site. In total 32 independent samples are included. Figure 5 illustrates the agreement between model-interpreted crown closure and ground measurements. The coefficients of determination R^2 and root mean square error (RMSE) are equal

to 0.6 / 0.064 for QuickBird scaling-based method, and 0.51 / 0.048 for Hyperion PPI method respectively.

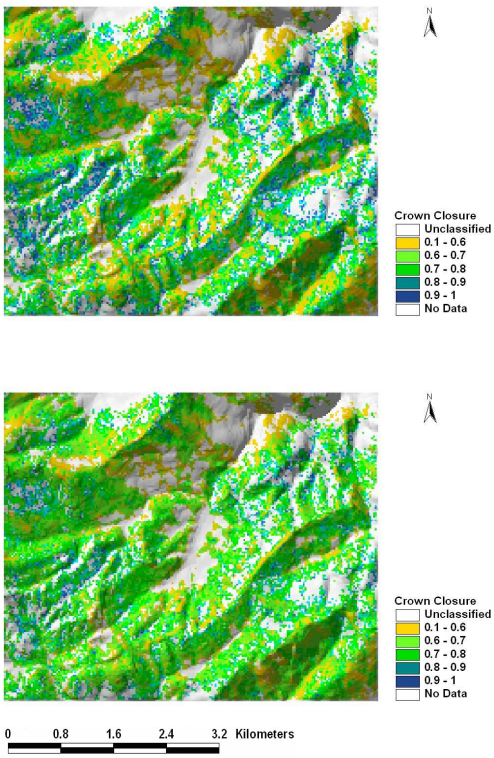

Figure 4. Mapping results of forest crown closure by the inverted geometric-optical model (Up: QuickBird scaling-based method; Down: Hyperion PPI method)

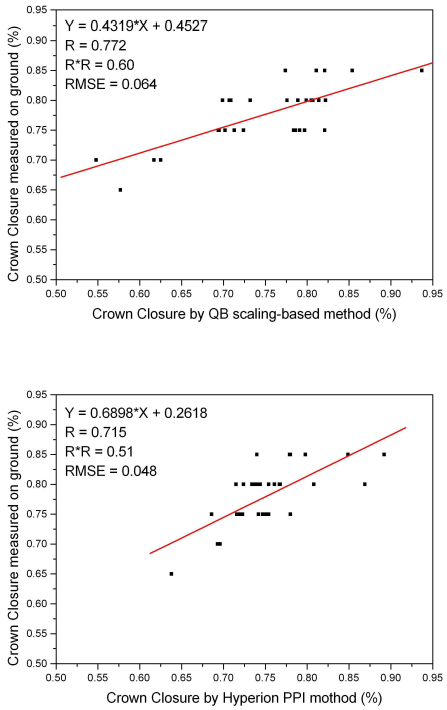

Figure 5. Linear relationship between ground measured CC and model derived CC

The validation results show that most of the model interpreted CC values are less than the ground measurements for both endmember extraction methods. But comparing the two methods, the results of QuickBird scaling-based method seem better than the pure-pixel deriving method in terms of the simulated regression lines.

6. CONCLUSION AND OUTLOOK

In this study, we use an inverted Li-Strahler geometric-optical model to retrieve one of the forest canopy variables (crown closure) from a hyperspectral Hyperion image collected in the Longmenhe broadleaved forest natural reserve, located in the Three Gorges region of China. For preparing the inverted model inputs, we compare two endmember extraction methods: linear spectral unmixing based technique, which requires a subset Hyperion image combined with the components' fractional images from the matched QuickBird high spatial resolution data, and another method by selecting the pure pixel directly from the Hyperion image. Depending on the comparison of derived endmember profiles and the validation of the model outputs with field measurements, we can conclude that the linear spectral unmixing based technique is an effective method to estimate the components' endmembers in a medium spatial resolution image. It can solve the mixed-pixel problem, when a matched high spatial resolution image is provided.

Since the collected QuickBird image of this case is smaller than the Hyperion image, only the overlapped region can be used for extracting the endmembers. However, if the overlapped region is including all components and it is located in a typical area of the Hyperion image, then the derived components' endmembers can be used for the whole Hyperion image. It indicates that the method of linear spectral unmixing based technique appears appropriate for up-scaling the information from high spatial resolution data, and it can also expand the consistent information from local to regional scale.

Although the endmember extraction method of linear spectral unmixing based technique is applied using QuickBird as high spatial resolution image and Hyperion as medium spatial resolution image in this study, it can be implemented for any two sets of data with different spatial and spectral resolution, such as from QuickBird to Landsat TM, from landsat TM to MODIS, and even from Hyperion to MODIS. Therefore, using this up-scaling method to explore the information from images at global scale is also feasible.

In future work, we will continue the study of quantitatively monitoring the forest canopy variables in the whole Three Gorges region of China using multi-scale and multi-spatial / spectral resolution data through the inverted Li-Strahler geometric-optical model and the up-scaling method. Even though the processes of the inverted model and the scaling method will need more careful analysis and calibrations in the future, the presented results show confidence in the approach selected.

ACKNOWLEDGMENT

We gratefully acknowledge financial support from the 'Knowledge Innovation Project' of the Chinese Academy of Sciences (No. KZCX3-SW-334). We appreciate support from Xu Wenting, Huang Jianxi and Tian Yichen for participation in the field campaign.

REFERENCES

AIG, 2002. ACORN 4.0 User's Guide, Boulder, CO: Analytical Imaging and Geophysics LLC.

Baatz, M. et al., 2004. eCognition Professional User Guide 4. Definiens Imaging, Munich.

Beck, R., 2003. EO-1 User Guide - Version 2.3, Satellite Systems Branch, USGS Earth Resources Observation Systems Data Center (EDC).

Chopping, M., Su, L., Laliberte, A., Rango, A., Peters, D.P.C. and Kollikkathara, N., 2006. Mapping shrub abundance in desert grasslands using geometric-optical modeling and multi-angle remote sensing with CHRIS/Proba. Remote Sensing of Environment, 104(1): 62-73.

Franklin, J. and Strahler, A.H., 1988. Invertible Canopy Reflectance Modeling of Vegetation Structure in Semiarid Woodland. Ieee Transactions on Geoscience and Remote Sensing, 26(6): 809-825.

Gemmell, F., 1999. Estimating conifer forest cover with thematic mapper data using reflectance model inversions and two spectral indices in a site with variable background characteristics. Remote Sensing of Environment, 69(2): 105-121.

Gerard, F.F. and North, P.R.J., 1997. Analyzing the effect of structural variability and canopy gaps on forest BRDF using a geometric-optical model. Remote Sensing of Environment, 62(1): 46-62.

Goodwin, N., Coops, N.C. and Stone, C., 2005. Assessing plantation canopy condition from airborne imagery using spectral mixture analysis and fractional abundances. International Journal of Applied Earth Observation and Geoinformation, 7(1): 11-28.

Green, A.A., Berman, M., Switzer, P. and Craig, M.D., 1988. A Transformation for Ordering Multispectral Data in Terms of Image Quality with Implications for Noise Removal. Ieee Transactions on Geoscience and Remote Sensing, 26(1): 65-74.

Haertel, V.F. and Shimabukuro, Y.E., 2005. Spectral linear mixing model in low spatial resolution image data. Ieee Transactions on Geoscience and Remote Sensing, 43(11): 2555-2562.

Hall, F.G., Shimabukuro, Y.E. and Huemmrich, K.F., 1995. Remote-Sensing of Forest Biophysical Structure Using Mixture Decomposition and Geometric Reflectance Models. Ecological Applications, 5(4): 993-1013.

Han, T., Goodenough, D.G., Dyk, A. and Love, J., 2002. Detection and correction of abnormal pixels in hyperion images, IGARSS, pp. 1327-1330.

Li, X. and Strahler, A., 1992. Geometric-optical bidirectional reflectance modeling of the discrete crown vegetation canopy: Effect of crown shape and mutual shadowing. Ieee Transactions on Geoscience and Remote Sensing, 30: 276-292.

Li, X. and Strahler, A.H., 1985. Geometric-optical modeling of a conifer forest canopy. IEEE Transactions on Geoscience and Remote Sensing, GE-23(5): 705-721.

Li, X. and Wang, J., 1995. vegetation Optical Remote Sensing Models and Vegetation Structure Parameterization. Science Press, Beijing, 118 pp.

Liang, S., 2004. Quantitative remote sensing of land surfaces. Wiley series in remote sensing. Wiley-Interscience, Hoboken, NJ, XXVI, 534 pp.

McKnight, T.L. and Hess, D., 2000. Climate Zones and Types: Dry Humid Subtropical Climate (Cfa, Cwa). Physical Geography: A Landscape Appreciation. Upper Saddle River, NJ: Prentice Hall, 223-6 pp.

Peddle, D.R., Franklin, S.E., Johnson, R.L., Lavigne, M.B. and Wulder, M.A., 2003. Structural change detection in a disturbed conifer forest using a geometric optical reflectance model in multiple-forward mode. Ieee Transactions on Geoscience and Remote Sensing, 41(1): 163-166.

Peddle, D.R., Hall, F.G. and LeDrew, E.F., 1999. Spectral Mixture Analysis and Geometric-Optical Reflectance Modeling of Boreal Forest Biophysical Structure. Remote Sensing of Environment, 67(3): 288-297.

Plaza, A., Martinez, P., Perez, R. and Plaza, J., 2004. A quantitative and comparative analysis of endmember extraction algorithms from hyperspectral data. Ieee Transactions on Geoscience and Remote Sensing, 42(3): 650-663.

Scarth, P. and Phinn, S., 2000. Determining Forest Structural Attributes Using an Inverted Geometric-Optical Model in Mixed Eucalypt Forests, Southeast Queensland, Australia. Remote Sensing of Environment, 71(2): 141-157.

Scarth, P., Phinn, S. and McAlpine, C., 2001. Integrating high and moderate spatial resolution image data to estimate forest age structure. Canadian Journal of Remote Sensing, 27(2): 129-142.

Schaaf, C.B., Li, X.W. and Strahler, A.H., 1994. Topographic Effects on Bidirectional and Hemispherical Reflectances Calculated with a Geometric-Optical Canopy Model. IEEE Transactions on Geoscience and Remote Sensing, 32(6): 1186-1193.

Strahler, A.H. and Jupp, D.L.B., 1990. Modeling Bidirectional Reflectance of Forests and Woodlands Using Boolean Models and Geometric Optics. Remote Sensing of Environment, 34(3): 153-166.

Woodcock, C.E., 1994. Estimation of forest stand structure from Landsat TM through inversion of the Li-Strahler model, IGARSS, pp. 1245-1247.

Woodcock, C.E., Collins, J.B., Gopal, S., Jakabhazy, V.D., Li, X., Macomber, S., Ryherd, S., Judson Harward, V., Levitan, J., Wu, Y. and Warbington, R., 1994. Mapping forest vegetation using Landsat TM imagery and a canopy reflectance model. Remote Sensing of Environment, 50(3): 240-254.

Woodcock, C.E., Collins, J.B., Jakabhazy, V.D., Li, X., Macomber, S.A. and Wu, Y., 1997. Inversion of the Li-Strahler canopy reflectance model for mapping forest structure. IEEE Transactions on Geoscience and Remote Sensing, 35(2): 405-414.

Zeng, Y., Schaepman, M.E., Wu, B., Clevers, J.G.P.W. and Bregt, A.K., 2007. Forest Structrual Variables Retrieval Using EO-1 Hyperion Data in Combination with Linear Spectral Unmixing and an Inverted Geometric-Optical Model. Journal of Remote Sensing - Special Issue of ISPMSRS05, 11(5): in press.

Zhukov, B., Oertel, D., Lanzl, F. and Reinha?ckel, G., 1999. Unmixing-based multisensor multiresolution image fusion. IEEE Transactions on Geoscience and Remote Sensing, 37(3 I): 1212-1226.

Zurita-Milla, R., Clevers, J.G.P.W. and Schaepman, M.E., 2006. Landsat TM and MERIS FR image fusion for land cover mapping over the Netherlands. Proceedings of the 2nd Workshop of the EARSeL SIG on Land Use and Land Cover: 34-40.